PCCP
Physical Chemistry Chemical Physics

Accepted Manuscript

This article can be cited before page numbers have been issued, to do this please use: J. K. Bediako, *Phys. Chem. Chem. Phys.*, 2026, DOI: 10.1039/D6CP00058D.

ROYAL SOCIETY OF CHEMISTRY

rsc.li/pccp

View Article Online
DOI: 10.1039/D6CP00058D

Post-synthesis functionalization of KOH-activated carbon with quaternary ammonium moiety for improved adsorption of monovalent gold

John Kwame Bediako*

Department of Separation Science, School of Engineering Science, Lappeenranta-Lahti University of Technology (LUT), FI-53850, Lappeenranta, Finland

*Corresponding author. E-mail address: john.bediako@lut.fi (J. K. Bediako)

View Article Online
DOI: 10.1039/D6CP00058D

Abstract

Activated carbon (AC) has been widely applied for gold recovery and remains the most preferred adsorbent, owing to its good physicochemical and adsorption properties. Among various available activation agents, KOH is reported to produce ACs with high yields, well-defined pore sizes, ultra-high specific surface areas and high reactivities. In this study, post-synthesis functionalization of KOH-AC with a quaternary ammonium moiety was carried out with the aim of converting an agro waste precursor into a high-value AC and improving the adsorption efficiency for monovalent gold contained in potassium dicyanoaurate (1) complex, i.e., $K[Au(CN_2)]$, via an environmentally friendly approach. The synthesis process commenced with pre-carbonization and activation under nitrogen environment, followed by chemical functionalization. The crystallinity, pore structure, atomic energy binding states and Au(I) loading capacity were investigated through characterization and batch adsorption studies. The experimental maximum equilibrium adsorption capacity was 513.52 ± 18.52 mg/g, however, this may further reach 749.28 ± 34.79 mg/g, according to the Langmuir isotherm model. Finally, it was possible to regenerate the spent AC with a mixture of 1 M KCN and NaOH, making it potentially suitable for application on a larger scale.

Keywords: Activated carbon; KOH activation; Amine functionalization; Characterization; Aurocyanide adsorption

View Article Online
DOI: 10.1039/D6CP00058D

1. Introduction

Gold, Au is a chemical element which in its purest form, is bright, slightly reddish-yellow, dense, soft, malleable, and ductile. It often occurs as nuggets or grains in rocks, veins and alluvial deposits, or in a series of mixtures with silver [1-2]. It also naturally alloys with copper and palladium [3]. Au is very precious to the manufacturing and high-tech industries, as it finds unlimited applications in the areas of automobile, health, coinage, jewelry, catalysis, sensing, electric and corrosion resistance [4-7]. Conventional Au mining from auriferous ores involves cyanidation in the presence of oxygen, carbon adsorption and leaching stages in industrial carbon-in-pulp (CIP) and carbon-in-leach (CIL) plants [8-10]. Although modern separation and purification technologies, including solvent extraction using organic eluents and ion exchange using polymeric resins are being championed, recent research has shown that activated carbon (AC) is both efficient in recovering Au from cyanide complexed solutions and chloro-complex-based metallurgical leachates [7, 11]. In a typical CIP plant, the pulp is made to flow through several agitated tanks where sodium cyanide and oxygen are added to dissolve the gold into solution, which is then channeled through adjoining agitated tanks containing AC. The Au, in the form of Au-cyanide complex, $[Au(CN)_2]^-$ is loaded onto the AC, which flows countercurrent to the dissolved pulp, while screens are placed to separate the barren pulp from the Au-laden AC [8-10, 12]. Eventually, the Au is leached in a heated mixture of sodium hydroxide and cyanide solution and recovered through an electrochemical refining or electroplating process [8, 10, 12]. The adsorption stage using granular AC is thus an important phase in the Au recovery process from crushed ores.

AC is described as a type of porous material that has been designed to have small, low-volume internal pores that increase the surface area available for adsorption and chemical reactions [7, 12-13]. It has been extensively applied in the age-long conventional CIP and CIL

View Article Online
DOI: 10.1039/D6CP00058D

processes for Au recovery and still remains the most preferred adsorbent owing to its good adsorption properties, such as high capacity, good affinity, fast kinetics and good chemical stability [14-17]. It has been established that the nature of carbon precursors, activation conditions and functional groups adversely affect the textural properties and chemical reactivities of the synthesized ACs [7, 18-19]. Large functional surfaces enhance the adsorbent–adsorbate interactions and hence, lead to higher adsorption capacities. In addition, high structural porosities permit easy migration of adsorbates into the inner adsorption sites, consequently improving the adsorption rates [18, 20]. Therefore, chemical activation using suitable activation agents, such as hydrogen peroxide, potassium hydroxide, sodium hydroxide, zinc chloride, sulfuric acid and phosphoric acid have been highly studied in efforts to augment the adsorption performances of ACs [21-23].

Among the afore-mentioned reagents, KOH is reported to produce ACs with high yields, well-defined pore sizes and ultra-high specific surface areas reaching over 1500 m^2/g, which are comparable to those of commercial ACs [23-26]. Besides, KOH activation is relatively cheaper and promising because higher activation can be achieved even at relatively lower activation temperatures, thereby encouraging environmentally sustainable production [18]. Moreover, it is relatively safer when compared to corrosive agents like $ZnCl_2$, which can pose hazards during the activation process, and requires careful handling and energy-intensive washing step to remove the residual $ZnCl_2$ and other impurities [27-28]. The KOH activation process progresses through various phases of interaction with C (carbon), such as decomposition, gasification and etching of the carbon framework by redox reactions that lead to micro- and macro-pore formations [18, 29-30]. Furthermore, KOH is known to favor the generation of surface chemical groups, particularly oxygen-containing groups on the carbon surface, which can be engineered to suit specific applications, such as decolorization and

View Article Online
DOI: 10.1039/D6CP00058D

deodorization in the purification of water, reduction of chlorine, protection of acid rain, and recovery of volatile organic compounds [12, 18, 31].

In previous studies, the contributions of nitrogen-containing groups, predominantly graphitic and quaternary-N groups to the overall adsorption of aurocyanide at alkaline pH were observed [7, 17]. With the above observations in mind, post-synthesis functionalization of the synthesized AC with quaternary ammonium groups was expected to significantly boost the adsorption capacity, since these groups can maintain their positive charges in a wide range of pH [32-34]. In fact, the modification of AC with functional moieties has been observed to markedly enhance the aurocyanide adsorption performances of synthesized ACs [35-36]. For example, Vargas *et al*. reported the immobilization of anionic surfactant, sodium dodecylsulfate (SDS) into a granular AC and observed a 10% improvement in the aurocyanide adsorption [35]. In addition, using high-sulfur petroleum coke as the raw material, Ramírez-Muñiz *et al*. prepared sulfur-impregnated AC (SIAC) that exhibited an improved aurocyanide adsorption capacity of 126.77 mg/g [36].

In this study, therefore, orange peel AC (OPAC) was first synthesized according to the previous reports [7, 17]. Next, post-synthesis functionalization of the OPAC with the quaternary ammonium moiety, (3-Chloro-2-hydroxypropyl) trimethyl ammonium chloride (CHPTAC), was carried out. Orange is one of the most favored subtropical fruits in the world, with its primary use being eating as fresh (cut) fruit or as food complement in desserts, salads, gelatins, fruit cocktails, jam or juice combinations in the citrus processing industries [29, 37]. The global production of orange was projected by the Food and Agriculture Organization (FAO) to hit some 64 million metric tons in the past decade [29, 38]. With the peel occupying nearly half of the total fruit weight, this figure translates into about 32 million metric tons of orange peels being generated as waste [29]. Hence, orange peel (OP) as a precursor for AC

View Article Online
DOI: 10.1039/D6CP00058D

synthesis can be cheaply and readily obtained, and it offers a strategic advantage for reducing environmental pollution. CHPTAC has been widely employed in cationization reactions to chemically modify the functionalities of materials for various applications. For instance, a novel polymeric flocculant was prepared by chemical insertion of CHPTAC and used to remove both positively and negatively charged contaminant particles in suspensions [39]. In addition, dye adsorption was performed on low-cost fibrous cellulose materials subjected to a cationization process using CHPTAC [40]. Furthermore, CHPTAC-anchored AC was produced from commercial AC by epoxide-induced method and used for improved removal of Cr(VI) [34]. Nonetheless, no report exists so far for the application of CHPTAC-functionalized AC for aurocyanide adsorption.

The aim of this study is, therefore, to valorize low-cost waste OP into an eco-friendly adsorbent and to further improve the adsorption capacity significantly by introducing cationic functionality that could interact with and capture anionic aurocyanide complex, $[Au(CN)_2]^-$. This is to be achieved through a post-synthesis functionalization process whereby the surface hydroxyl groups of synthesized KOH-activated OPAC would react with the CHPTAC moiety via a cationization reaction in alkaline solution and under controlled heat. This chemical treatment would ultimately lead to a remarkable improvement in the physicochemical properties and aurocyanide adsorption capacity of the eventual quaternary amine-functionalized OPAC.

2. Materials and methods

2.1. Materials

The OP precursor was randomly collected from orange sellers in the eastern region of Ghana, cleaned, dried and stored for use. All the chemicals used in this study were of analytical

View Article Online
DOI: 10.1039/D6CP00058D

grades and were used as received without further purification. The CHPTAC reagent (60 wt. % in H_2O, liquid) and potassium dicyanoaurate(1), $K[Au(CN)_2]$ (purity: 98%) were purchased from Sigma–Aldrich. Besides, NaOH, KOH and HCl were procured from Daejung Chemicals and Metals Co., Ltd. (Gyonggi-do, Korea), and double distilled water (DW) was obtained from a Direct-Q UV Millipore dispenser, Merck Millipore.

2.2. Methods

Grounded OPs passing through a 2 mm aperture but retaining on a 0.35 mm aperture mesh (standard testing sieves, Chung Gye Sang Gong SA., Seoul, Korea) were pre-carbonized in an automated furnace maintained at 400 °C for 1 h under constant N_2 supply [17]. The pre-carbonized OPs were impregnated with 4 M KOH in the ratio of 2:1 (KOH:pre-carbonized OP, wt./wt.) for 3 h and activated at 800 °C for 1 h, also under N_2 purging. The now OPACs were washed and oven-dried at 70 °C for 24 h. Approximately 2 g of the OPACs were dispersed in 50 mL of DW and pH adjusted to >10 using 1 M NaOH. The content in a round-bottom flask was placed in an oil bath kept at 60 °C for ~2 h under stirring using a magnetic bar, and then 1 mL of CHPTAC was gently added to initiate the cationization reaction as shown in Fig. 1. After 24 h, the reaction was stopped and the quaternary amine-functionalized ACs (A-OPACs) were washed thoroughly with DW and separated by means of a vacuum filter system. Finally, the filtered samples were oven-dried at 70 °C for 24 h, characterized using different instrumental analyses, and used for Au(I) adsorption from potassium dicyanoaurate(1).

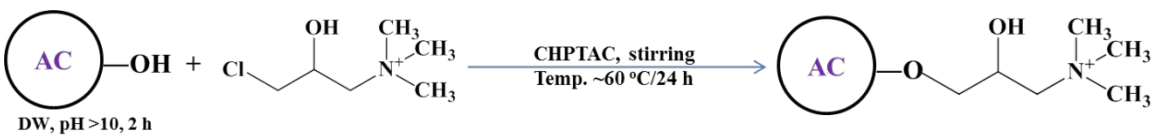

Fig. 1. Illustration of the cationization reaction between OPAC and CHPTAC.

View Article Online
DOI: 10.1039/D6CP00058D

2.3. Characterization of the synthesized A-OPACs

The surface morphology and elemental compositions of the synthesized A-OPACs were examined using a combined field emission scanning electron microscopy and energy disperse X-ray spectroscopy system (FE-SEM/EDX, SUPRA 40VP, Carl Zeiss, Germany). The samples were sputter coated with Pt prior to observation under the microscope to prevent surface charging [41]. Other instruments, including Fourier transforms infra-red (FTIR) spectrometer (PerkinElmer spectrophotometer: Spectrum GX, FTIR System), thermal analyzing equipment (TA Q600 DSC/TGA, TA Instruments, USA), X-ray diffractometer (XRD, multi-purpose high-performance X-ray diffractometer, X'pert Powder, PANalytical, the Netherlands), surface area and pore size analyzer (BELSORP-max BET equipment) and X-ray photoelectron spectroscopy, XPS equipment (AXIS-NOVA spectrometer, Kratos Analytical, Ltd., UK) were employed to fully analyze the physicochemical properties and mechanisms of aurocyanide adsorption.

2.4. Aurocyanide adsorption and regeneration studies

Adsorption isotherm and kinetic experiments were conducted to estimate the possible maximum capacity and rate of the A-OPAC for attaining adsorption equilibrium [42]. All the experiments were conducted in triplicates and the average values with standard errors are presented. The adsorption isotherm experiments were carried out in 50 mL falcon tubes with 0.02 g A-OPAC doses in 30 mL aurocyanide solutions of different concentrations ranging from 0–2000 mg/L. The contents were placed in a multi-shaking incubator maintained at 25 ± 2 ^{o}C and 140 rpm for 24 h. The pH of each solution was adjusted within the range of pH 10.5–11 to avoid formation of the toxic gas, HCN that often emits at acidic pH.

Alternatively, regeneration and reuse experiments were run to test potential recyclability of

View Article Online
DOI: 10.1039/D6CP00058D

the A-OPAC in multiple adsorption-desorption cycles. First, adsorption was conducted using 50 mg/L Au(I) solution, then the Au-loaded A-OPAC was separated from the residual solution by filtration and re-suspended in a 1 M mixture of KCN and NaOH (dosage: 0.02 g A-OPAC per 30 mL eluent solution) for desorption and regeneration as described for the adsorption step.

In the case of the kinetic experiment, 0.2 g of A-OPAC was added to 250 mL of 100 mg/L solution in a glass bottle placed on a magnetic stirrer with a bar at room temperature and 300 rpm. Aliquots of the solution were withdrawn at predetermined time intervals from the bulk for a period of 24 h. The drawn solutions were centrifuged and diluted for residual concentration analyses using an inductively coupled plasma-atomic emission spectrometer, Thermo Scientific, iCAP 7000 series, ICP Spectrometer, USA. The equilibrium uptakes, q were calculated using the expression in Eq. (1).

$$q = \frac{(C_i - C_e)V}{M} \quad (1)$$

where Ci and C_e are the initial and equilibrium concentrations in mg/L, V is the volume in L, and M is the dry mass in g. In situations where there was significant change in the volume, the difference between the final and initial volumes were considered.

3. Results and discussion

3.1. Characterization analysis

3.1.1 Morphological and elemental characterization

Surface morphologies of the OP and A-OPACs (before and after adsorption) were observed on the FE-SEM/EDX system at 20.00 KX (i.e., 20,000 magnifications). As evident from Fig. 2, the surface of the OP looked tender-rough and gummy without any noticeable pores.

View Article Online
DOI: 10.1039/D6CP00058D

However, the presence of numerous visible pores could be confirmed in the images of the A-OPAC before interaction with the aurocyanide solution. Filling of the Au(I) complex into the porous structures appeared to have marginally narrowed the pore sizes after adsorption (Fig. 2c and e). Expectedly, the carbon content increased considerably owing to escape of volatile components during the pyrolysis process which led to creation of the porous frameworks that were observed. EDX potentially confirms metal adsorption by detecting the presence of metal ions on the surface of the adsorbent both before and after the adsorption process [43-44]. That is, the presence of Au and K peaks in the EDX spectrum after adsorption showed evidence of adsorbed $K[Au(CN)_2]$ and $[Au(CN)_2]^-$ onto the A-OPAC. This observation is consistent with recent studies examining the adsorption of Cr(VI) onto activated charcoal synthesized from *Sida Acuta* plant leaves [43], and the removal of other heavy metal ions from aqueous solutions [45]. It must be noted, however, that the appearance of the Pt peaks in all the EDX patterns were due to the Pt used in sputter coating the surfaces before the analysis [41].

View Article Online
DOI: 10.1039/D6CP00058D

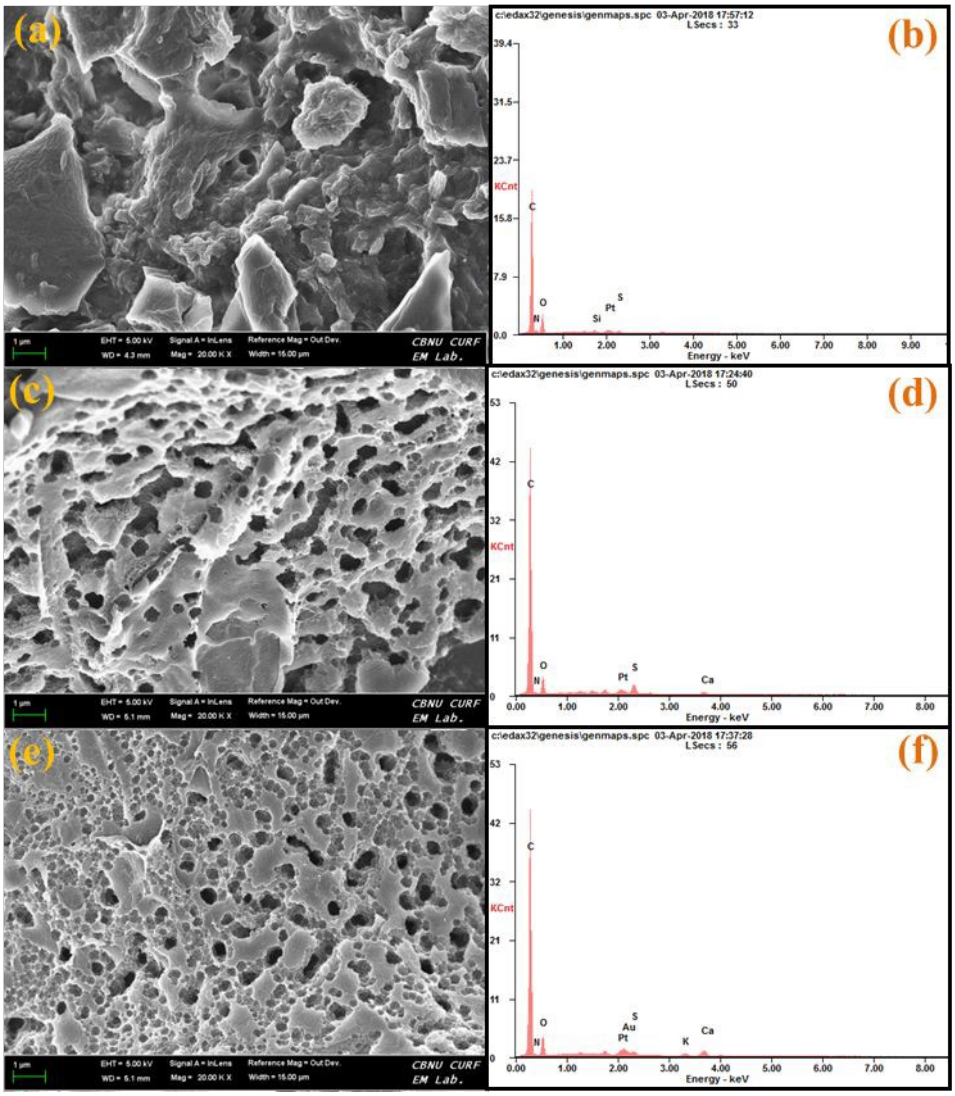

Fig. 2. Respective FE-SEM images and EDX elemental peaks of (a and b) OP, (c and d) A-OPAC and (e and f) gold loaded A-OPAC.

3.1.2 Crystallinity, textural and functional group characterization

The crystallinity of the A-OPAC was analyzed in the 2θ range of 10° – 80° (before and after adsorption). A broad hunch-like reflection attributable to the (002) reflection of a graphitic-type lattice was observed at 2θ = 24.5°, with a corresponding weak reflection centered around 43.5 ° (Fig. 3(a)). This may correspond to a superimposition of the (100) and (101) reflections of the graphitic-type carbon structure and thus indicate a limited degree of graphitization [46-49].

View Article Online
DOI: 10.1039/D6CP00058D

Noteworthily, the graphitic structure was not altered or destroyed even after the vigorous interactions of the ACs with the aurocyanide solution. Moreover, the non-appearances of characteristic face centered cubic lattice peaks representative of reduced Au indicate that the aurocyanide was potentially adsorbed in its monovalent state of $[Au(CN)_2]^-$ without any chemical changes [17, 50].

Furthermore, physical adsorption of gases is the most applied technique for the characterization of porous materials [51]. Therefore, the BET surface area and pore size distributions of the AC samples were examined through N_2 adsorption measurements. The adsorption isotherm plot in Fig. 3(b) shows a sharp uptake at very low relative pressure, followed by an early plateau with a closure at P/P_0 near 0.2. This is characteristic of a type-I isotherm curve and suggests the existence of micropores in the A-OPAC structures [52-53]. The inset of Fig. 3(b) shows the pore size distribution plot with a base covering 0.5–2.0 nm and a mean pore diameter at ~1.0 nm, confirming the presence of micropores in the structures of the A-OPAC.

Moreover, the surface functional groups were analyzed using the KBr disc technique in the wavelength range from 4000–400 cm^{-1}. The surface complexity of the pristine OP was identified with several absorption bands (Fig. 3(c)). Specifically, the peaks appearing at 3437, 2948, 2869, 1764, 1647, 1451, 1274, 1069 and 638 cm^{-1} were assigned to O–H stretching, C–H ($–CH_2$ and $–CH_3$) stretching of hydrocarbons, C=O stretching of carboxylic acids or esters, symmetric C=O stretching in COOH, asymmetric COO^- bending, C–H stretching, C–O stretching of esters or ethers and N–H deformation of amines, respectively [54-55]. Evidence of reduction in the surface complexity of the virgin biomass after burning off the volatile organic components was manifested by decrease in the number of absorption bands observed in the spectra of the ACs. The peaks emerging at 3457 cm^{-1} corresponded to pyrrolic-N and

View Article Online
DOI: 10.1039/D6CP00058D

O–H stretching, those at 1774 cm^{-1} were allocated to carboxyl stretching, and those at 1626 cm^{-1} were attributed to C=C stretching mode of the skeletal framework of sp^2 carbons and C–N stretching vibrations [41, 56]. These observations suggested effective carbonization, activation and amine-functionalization of the agro waste biomass sample.

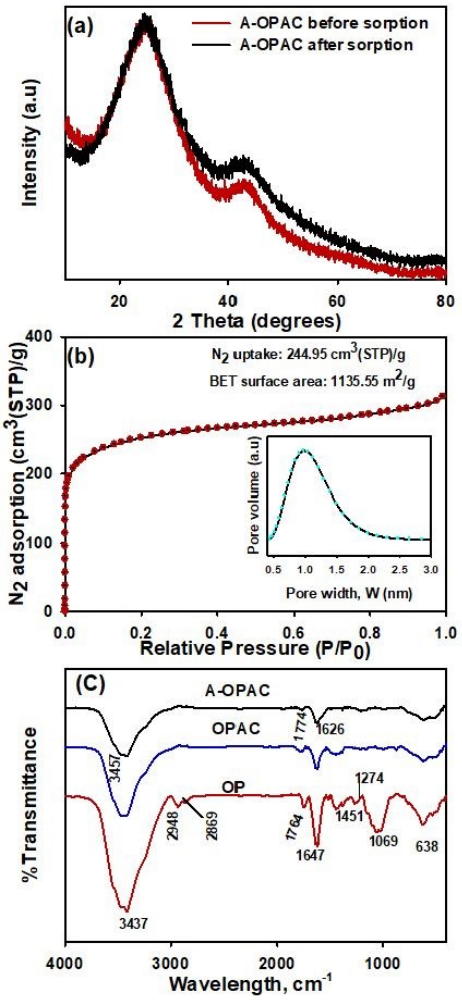

Fig. 3. (a) XRD patterns, (b) BET surface area and pore size distribution, and (c) FTIR spectral plots.

3.1.3 XPS characterization and mechanisms of aurocyanide adsorption

High resolution XPS spectra of the core-level C, N and Au atoms were separated and analyzed to assess the surface chemical composition of the samples and to understand the

View Article Online
DOI: 10.1039/D6CP00058D

mechanisms of aurocyanide adsorption. The core-level spectra for each of the pristine OP and A-OPAC (before and after adsorption) were deconvoluted into sub-components (Fig. 4). The most intense peaks for the C1s spectra were found at the binding energy of *ca.* 284 eV, which correspond to C=C and C–C in the carbon framework or C–H bonds in methyl and methylene (hydrocarbon) groups (Fig. 4(a)) [55, 57]. The rest of the peaks centered between 285 – 289 eV were respectively assigned to C–O, C–N, C=O, and O–C=O of carboxylic acids, alcohols, phenols, ethers and ester groups [55, 57-58]. Interestingly, a π–π* shake-up satellite peak had emerged at 290.63 eV in the spectrum of the A-OPAC. This peak had slightly shifted to 291.24 eV after adsorption, indicating its likely involvement in the adsorption process. In other words, the presence of π bonds in both the aurocyanide complex and the AC make π-π interaction a significant contributor to the adsorption process [7-8]. This observation also confirmed the non-destructive nature of the formed graphitic structure which was earlier spotted in the XRD diffraction patterns (Fig. 3(a)).

In the deconvoluted N1s spectra of the pristine OP, two peaks representing primary ($–NH_2$) and secondary (–NH–) amines from the amino acid groups in proteins were identified at 399.27 and 400.66 eV (Fig. 4(b)) [57, 59-60]. Conversely, the N1s spectra of the A-OPAC showed completely different sets of nitrogen-containing groups, suggesting successful pre-carbonization and activation, with an added advantage of N doping into the carbon framework. These N-bearing groups include amino-N (397.81/398.08 eV), pyrrolic-N (399.84/400.11 eV), graphitic-N/quaternary-N (402.21/402.23 eV) and nitrite, $–NO_2$ (404.44/405.72 eV) groups [17, 33, 41], which possibly stemmed from the nitrogen environment and amine-functionalization. It is purported that in the adsorption of aurocyanide in alkaline pH, O-containing functional groups do not have any positive effects due to the strong repulsive forces that exist between them and the anionic aurocyanide complex [50, 61-63]. It is

View Article Online
DOI: 10.1039/D6CP00058D

thus worthwhile to assume that the prevalence of the enormous N-containing groups may likely act as the main active sites for the adsorption of $[Au(CN)_2]^-$ via electrostatic interactions. Thus, the interactive interplay is proposed to be sequential, i.e., electrostatic interaction that draws the $[Au(CN)_2]^-$ complex onto the A-OPAC due to its positively charged surface, followed by π-π interaction between the π bonds existing in both the A-OPAC and $[Au(CN)_2]^-$ complex.

It must be noted that in analyzing the presence of adsorbed gold, the Au4f spectra was deconvoluted. An alternative approach would be to determine the signals of C≡N bond in the C1s and N1s spectra; however, the peak position of the C≡N bond is so close to the C=N and C–N peaks at around 285 – 286 eV for C1s and 399 – 400 eV for N1s, leading to possible overlapping of peaks [64-66]. Hence, the option of exploring the Au4f signals was found to be more reliable and straightforward. Consequently, the Au4f spectra of the OP and A-OPAC revealed no obvious peaks characteristic of adhering Au prior to adsorption (Fig. 4(c)). However, a pair of spin-orbit peaks were observed in the spectra of A-OPAC at $Au4f_{7/2}$ (84.89 eV) and $Au4f_{5/2}$ (88.54 eV) after adsorption, indicating successful adsorption and retention of the aurocyanide complex onto the A-OPAC [67]. Gold mainly exists in three oxidation states of 0, +1 and +3, with corresponding XPS binding energies close to 84.0, 85.0 and 86.0 eV ($Au4f_{7/2}$) [68-70]. Since the binding energy at 84.89 eV is closer to 85.0 eV, the adsorbed gold likely represents the monovalent species of Au(I). This result corroborates the XRD spectral analysis of the post-adsorption A-OPAC, which showed no traces of reduced gold, i.e., Au(0).

View Article Online
DOI: 10.1039/D6CP00058D

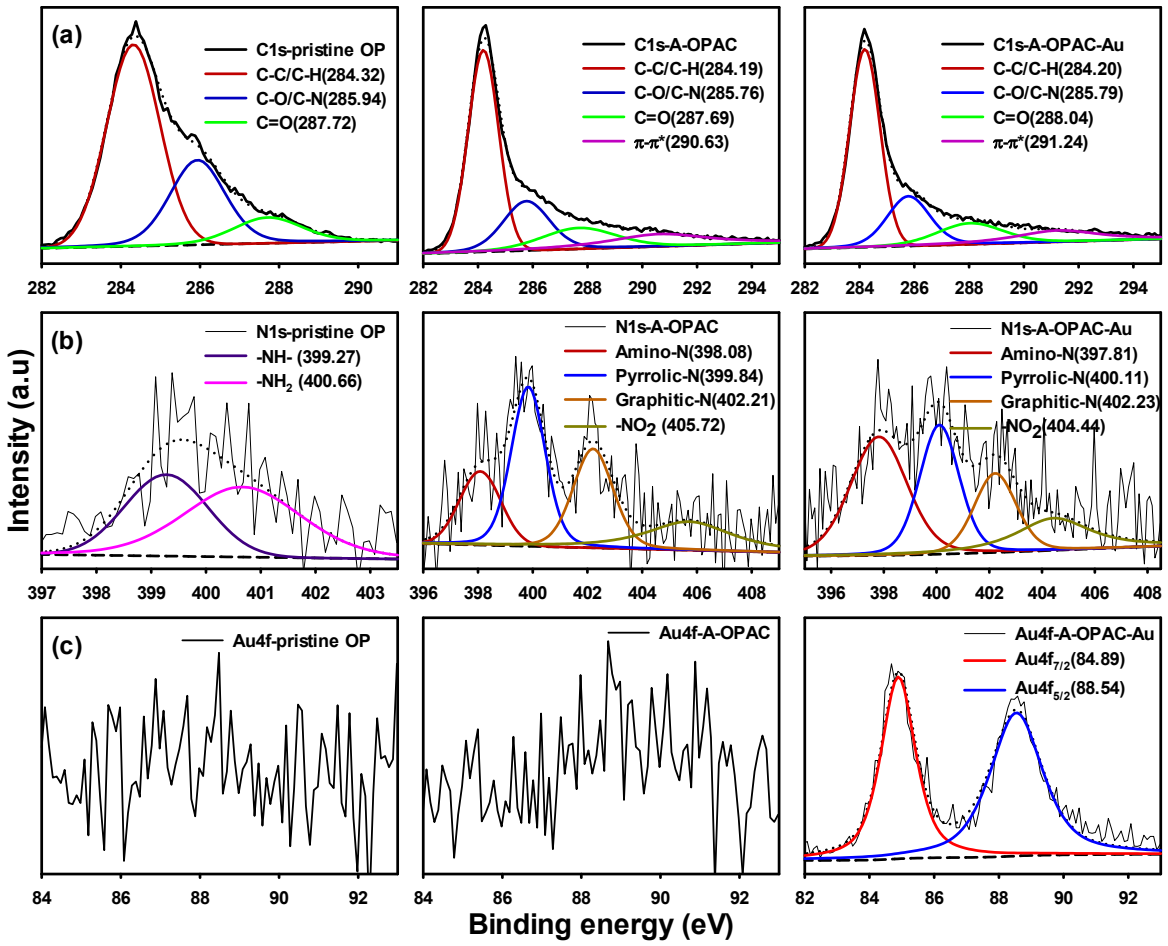

Fig. 4. Deconvoluted XPS of (a) C1s, (b) N1s and (c) Au4f core level spectra of OP and A-OPAC samples.

3.2. Adsorption studies

3.2.1 Design and reaction process of A-OPAC

Cationization of AC with CHPTAC occurs when CHPTAC reacts with the surface hydroxyl (–OH) groups on AC. Under alkaline conditions, the CHPTAC forms a reactive epoxide intermediate, glycidyltrimethylammonium chloride (GTAC), also known as 2,3-epoxypropyltrimethylammonium chloride (EPTAC), which then undergoes nucleophilic attack by the –OH groups on the surface of the AC (in this case A-OPAC). This opens the epoxide ring and covalently attaches the quaternary ammonium cation, (R_4N^+) onto the AC

View Article Online
DOI: 10.1039/D6CP00058D

surface [32, 71-72]. The result is a positively charged, cationic AC capable of enhanced adsorption of anionic species such as $[Au(CN)_2]^-$ (Fig. 1). Thus, the design process of the A-OPAC was such that the CHPTAC dosage for the cationic reaction was systematically varied at 0.2, 0.5 and 1 mL for a fix mass of 2 g OPAC. The preliminary adsorption evaluation showed increasing adsorption capacity with increasing CHPTAC dosage; however, this increment did not exactly commensurate with the changing dosage as depicted in Fig. 5(a). In other words, between 0.2 and 0.5 mL CHPTAC dosage, the aurocyanide uptake almost doubled, i.e., from ~65 to 115 mg/g. However, further increase in the dosage up to 1 mL, only led to a corresponding uptake of ~160 mg/g. Considering that doubling the CHPTAC dosage did not necessarily lead to a 2-fold increase in the aurocyanide uptake, the 1 mL CHPTAC was adopted as the limit dosage. With this dosage, the OP and pre-carbonized OP (OPC) were also functionalized with CHPTAC. The results in Fig. 5(b) show that the amine incorporation was markedly visible, reflecting in a corresponding increase in the adsorption capacities of the samples in the order of A-OP < A-OPC < A-OPAC. Moreover, all the CHPTAC-functionalized samples recorded appreciable boosts in their adsorption capacities as compared to their non-functionalized counterparts, i.e., OP, OPC and OPAC. This observation was not surprising since previous reports have shown improved adsorption affinity of modified ACs [35-36]. In fact, in the study involving sulfur impregnation of AC, it was explained that the sulfur on the surface of the modified AC had a strong linkage with the aurocyanide ions, hence demonstrating an enhanced aurocyanide adsorption capacity from 56.17 to 126.77 mg/g [36]. The role of AC surface functional groups in adsorption of cyano-complexes of Au and Cu was also investigated through density functional theory (DFT) and it was concluded that the presence of functional groups such as OH and COOH increased the adsorption tendency for both Au and Cu [73].

View Article Online
DOI: 10.1039/D6CP00058D

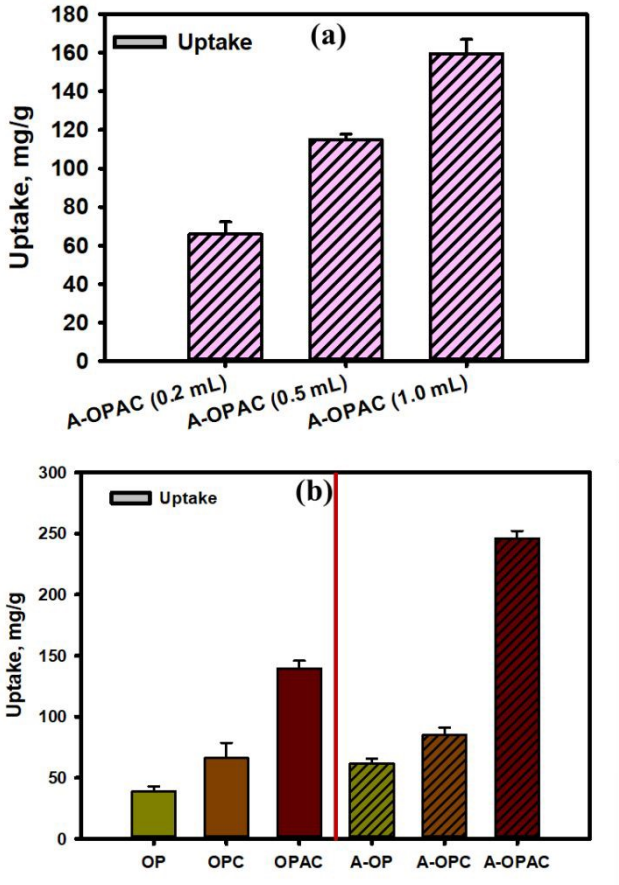

Fig. 5. Design process of A-OPAC. (a) Functionalization of OPAC with different doses of CHPTAC and corresponding aurocyanide adsorption evaluation. The values in braces show the volume of CHPTAC used. (b) Comparison of adsorption capacities of functionalized and non-functionalized samples. Experimental conditions: initial concentration: (a) ~250 mg/L and (b) ~500 mg/L; 0.02 g adsorbent dose /30 mL aurocyanide solution, time: ~48 h; pH: ~10.5-11.

3.2.2 Adsorption kinetics and intra-particle diffusion studies

Adsorption kinetic study is necessary for the design of adsorption systems for possible large-scale applications [74-75]. In this study, the kinetics experiment was conducted from 0–24 h during which sample solutions were timely drawn from the bulk phase, centrifuged and

View Article Online
DOI: 10.1039/D6CP00058D

diluted for analyses. From Fig. 6 (a), it could be seen that the adsorption rate was fast and reached equilibrium within ~1 h. For an AC, this is a commendable adsorption kinetics since most AC-based adsorption equilibria are reached in longer hours (Table 1). The obtained data were regressed in a SigmaPlot software (version 12.0, SPSS, USA) and fitted with the pseudo-first-order (PFO) and pseudo-second-order (PSO) kinetic models given by Eq. (2) and Eq. (3) [76-77]:

$$\text{Pseudo-first-order (PFO):}\quad q_t = q_{e1}(1 - exp\,(-k_1\,t)) \tag{2}$$

$$\text{Pseudo-second-order (PSO):}\quad q_t = \frac{q_{e2}^2 k_2 t}{1 + q_2 k_2 t} \tag{3}$$

where q_{e1} and q_{e2} are the equilibrium uptakes (mg/g); q_t is the adsorption amount at a given time, t (mg/g); k_1 is the first-order equilibrium rate constant (min^{-1}), and k_2 is the second-order equilibrium rate constant (g/mg min). The model results are summarized in Table 2. The PSO model presented better fitting of the data with a very high coefficient of determination, R^2 value of 0.997, as compared to the PFO model with an R^2 value of 0.973. Moreover, the equilibrium uptake, q_{e2} estimated from the PSO model was much more comparable to the experimental uptake, $q_{exp't}$ (Table 2).

Furthermore, the kinetic data were examined with the intra-particle diffusion (IPD) model expressed in Eq. (4).

$$\text{IPD model:}\quad q_t = k_i t^{0.5} + C_i \tag{4}$$

where k_i corresponds to the IPD rate constant and C_i represents the thickness of the boundary layer [75, 78-79]. IPD follows film diffusion and involves the diffusive migration of adsorbate from the adsorbent's surface deeper into the internal pores of the adsorbent. Film and particle

View Article Online
DOI: 10.1039/D6CP00058D

diffusion are thus the two main factors that control the rates of adsorption from liquid media by porous ACs [78]. Eq. (4) assumes that if IPD is involved in the adsorption process, then the plot of q_t versus $t^{0.5}$ must be linear [75, 78-79]. The plot shown in Fig. 6(b) with parameters in Table 3 revealed that two types of mechanisms may exist. In other words, there were two linear lines; the first line representing the initial rapid adsorption phase facilitated by the film diffusion and subsequent external surface coverage by the aurocyanide, and the second part being characterized by transportation of the adsorbate from the surfaces of the A-OPAC into the internal pores. Because the relationship plot of q_t versus $t^{0.5}$ was not linear for the full range of the contact time, IPD could not be considered the rate-limiting step for the entire kinetic regime, but only for the initial period of the adsorption process [78, 80]. Therefore, the aurocyanide adsorption onto the A-OPAC consisted of surface adsorption and IPD mechanisms; the surface adsorption functionality being likely enhanced by the amine modification of the AC surface with CPHTAC.

398 **Table 1** Comparison of aurocyanide adsorption performances of reported ACs.

Precursor/brand	Activation method	Activation temperature	Textural properties (surface area, pore volume)	Adsorption capacity (mg/g)	Kinetics	Ref.
Orange peel	Chemical activation with KOH	800 °C	1135.55 m^2/g, 244.95 cm^3/g	749.28± 34.79	PSO, R^2 0.997, 1 h	This work
Palm kernel shells	Physical activation with steam	900 °C	-	-	5 h	81
Commercial carbon	Solvothermal treatment using Fe_3O_4	-	249.7 m^2/g, 0.14 cm^3/g	45.2	PSO, R^2 0.999, 2 h	82
Norit C-Gran AC	Chemical activation with H_3PO_4	-	1565.2 m^2/g	362.11 ± 31.07	PSO, R^2 0.970, 2 h	7
Granular activated carbon	Surfactant impregnation using sodium dodecyl sulfate (SDS)	-	807.8 m^2/g, 0.39 cm^3/g	-	PFO, ~80% in 10 h	35
Orange peel	Chemical activation with $ZnCl_2$	800 °C	1439.5 m^2/g	660.72 ± 51.64	PSO, R^2 0.990, 4 h	7
Palm nut shells	Physical activation using steam	900 °C	903.1 m^2/g, 0.542 cm^3/g	63.04	12 h	81
Orange peel	Chemical activation with KOH	450–650 °C	-	97.8	-	83
Peach stone	Chemical activation with $ZnCl_2$	300–800 °C	503–805 m^2/g	13.1	PSO, R^2 0.997, 2 h	84
Macadamia nut shells	Physical activation using CO_2	800–1100 °C	173–602 m^2/g, 0.402 cm^3/g	-	40 h	12
Coal	Physical activation using steam	700–850 °C	427–773 m^2/g	9.35	-	85
Orange peel	Physical activation using KOH	535 °C	1098.80 m^2/g, 0.637 cm^3/g	186.95	PSO, R^2 0.988, 20 h	17
Haycarb AC	Physical activation with steam	-	1056.7 m^2/g	429.14 ± 44.53	PSO, R^2 0.950, 20 h	7
NORIT GAC 1240	Physical activation with steam	-	0.65 mm (effective size)	4406 g/ton	24 h	3

399

400

View Article Online
DOI: 10.1039/D6CP00058D

Table 2 Parameters of the pseudo-1st-order and pseudo-2nd-order kinetic models.

	Pseudo-1st-order			Pseudo-2nd-order		
$q_{exp't}$ (mg/g)	q_1 (mg/g)	k_1 (1/min)	R^2	q_2 (mg/g)	k_2 (g/mg min)	R^2
56.02±1.48	53.01±1.19	8.01±1.02	0.973	55.21±0.42	0.23±0.01	0.997

Table 3 Parameters of the intra-particle diffusion model of the kinetics data.

Phase	k_i (mg/g min$^{0.5}$)	C_i	R^2
1st	64.29±4.91	5.40±0.46	0.934
2nd	1.06±0.12	51.28±0.68	0.963

3.2.3. Adsorption isotherm and reuse studies

Adsorption isotherm experiments are useful for determining the amounts of adsorbents needed to effectively capture targeted amounts of adsorbates [75, 86]. Hence, the adsorption isotherm of the A-OPAC was conducted by adjusting the aurocyanide solutions of different concentrations to alkaline pH until equilibria were attained. The plot of equilibrium uptake, q_e verses equilibrium concentration, C_e showed that the amount of Au(I) adsorbed increased as the equilibrium concentration increased (Fig. 6(c)). As is the case for most adsorption processes, the adsorption affinity, b, was high at lower concentrations and diminished gradually with increasing equilibrium concentration. The adsorption capacity was, however, higher at higher concentrations and although the usual plateau-like shape was not achieved, equilibrium was fairly predicted by fitting the data through the Langmuir [87] and Freundlich [88] isotherm models. The equations for these models are presented in Eq. (5) and Eq. (6). From the models, the maximum adsorption capacity and dynamics of adsorption were estimated.

Langmuir model: $q_e = q_m \frac{bC_e}{1+bC_e}$ (5)

View Article Online
DOI: 10.1039/D6CP00058D

Freundlich model: $q_e = KC_e^{1/n}$ (6)

where q_e (mg/g), C_e (mg/L) and b (L/mg) have already been defined, q_m is maximum uptake at equilibrium (mg/g), K and n are the Freundlich constants denoting the relative adsorption capacity and adsorption intensity, respectively. The model results are summarized in Table 4. Compared to the Langmuir model, the data was less fitted to the Freundlich model; however, the K and n values obtained indicated a very good adsorptive interaction between the Au(I) solution and A-OPAC [78, 89]. From the Langmuir model, the maximum equilibrium uptake was calculated to be 749.28± 34.79 mg/g at an R^2 value of 0.994, significantly higher than the experimental uptake of 513.52±18.52 as would be expected. As can be seen from Table 1, a comparison of the aurocyanide adsorption performances of reported ACs revealed that both the experimental and predicted adsorption capacities of the present study are higher than most of the reported cases.

Table 4 Experimental and modeled isotherm data for the aurocyanide adsorption.

	Langmuir Model			Freundlich Model		
$q_{exp't}$ (mg/g)	q_{max} (mg/g)	b (L/mg)	R^2	k (L/g)$^{1/n}$	N	R^2
513.52±18.52	749.28±34.79	0.004±0.0003	0.994	8.24±0.78	1.75±0.04	0.998

Regeneration and reuse of spent ACs is a key step in the CIP/CIL processes, as it cuts down the amount of AC required to feed into new streams. This is important for reducing the operational costs and hence, boosting economic returns. Therefore, the A-OPAC was subjected to repeated adsorption-desorption cycles using 50 mg/L aurocyanide solution and 1 M eluent mixture of KCN and NaOH. After adsorption, the solution was gently filtered to separate the Au-loaded A-OPAC from the residual solution. Re-immersion was then done for desorption and regeneration in a multi-shaking incubator kept at 25 ± 2 °C and 140 rpm for

View Article Online
DOI: 10.1039/D6CP00058D

24 h. Overall, the regeneration and reuse efficiencies were good, and while the adsorption capacity decreased slightly to about 95% of the initial value due to potentially unavoidable adsorbent losses, 100% desorption efficiency was achieved throughout the four cycles (Fig. 6(d)).

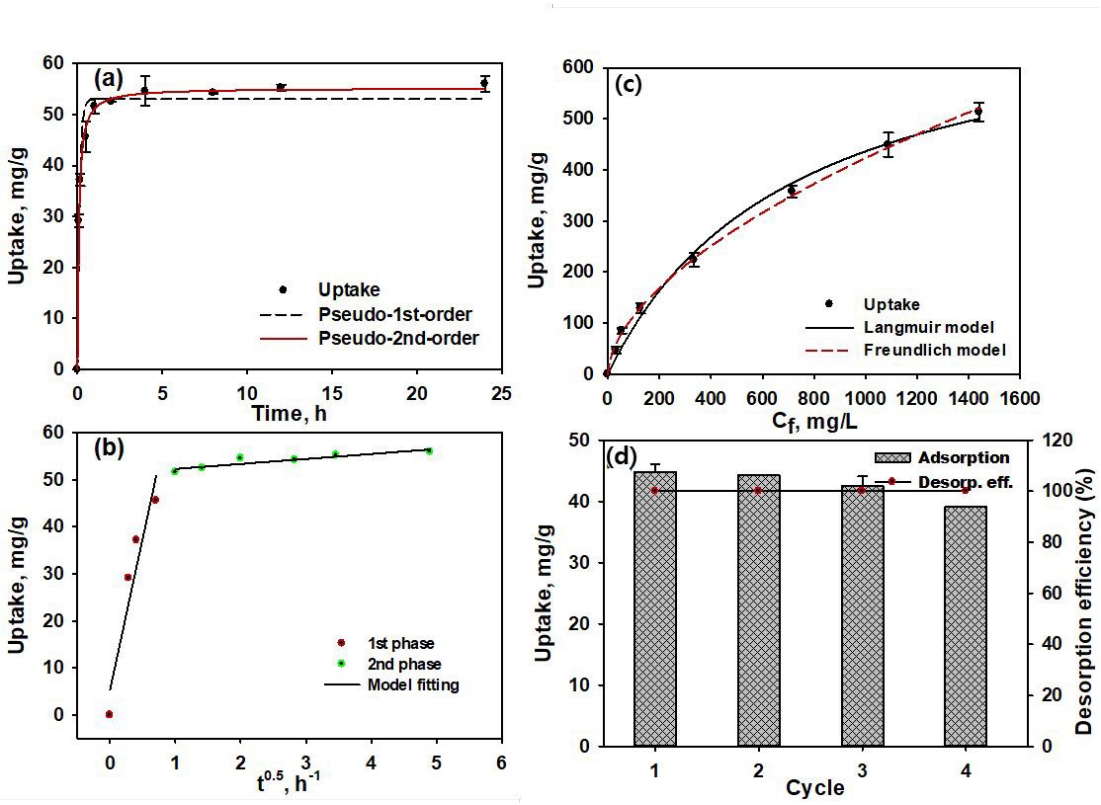

Fig. 6. Adsorption kinetics fitted to (a) PFO and PSO models and (b) IPD model. Experimental conditions: initial concentration: ~100 mg/L; time: ~0–24 h. (c) Adsorption isotherm evaluation, experimental conditions: initial concentration: ~0-2000 mg/L; 0.02 g A-OPAC dose/30 mL aurocyanide solution, time: ~48 h; pH: ~10.5-11 and (d) adsorption-desorption cycles of A-OPAC: ~50 mg/L, 0.02 g A-OPAC dose/30 mL 1 M KCN/NaOH mixture.

4. Conclusions

View Article Online
DOI: 10.1039/D6CP00058D

OP-derived KOH-AC was successfully synthesized and further functionalized with quaternary ammonium-containing CHPTAC via a cationization reaction. Successful amine incorporation was confirmed through instrumental analysis and aurocyanide adsorption experiments. The adsorption capacity of the A-OPAC towards Au(I) showed marked improvement from the pristine samples. The improvement in the adsorption capacity was attributed to the ability of the quaternary amine groups in CHPTAC to remain positively charged over a wide range of pH, including alkaline pH, thereby effectively undergoing electrostatic interactions with the anionic $[Au(CN)_2]^-$ complex. Thus, the adsorption process proceeded through surface adsorption and IPD mechanisms mainly via electrostatic and π–π interactions. The PSO model better described the kinetic data, and the Langmuir model fitted well to the isotherm data with an estimated maximum equilibrium Au(I) uptake of 749.28± 34.79 mg/g at 0.994 R^2 value. The significantly higher adsorption capacity and relatively fast kinetics (approx. 1 h equilibrium time), indicates that only a small amount of the A-OPAC is required to recover large amount of aurocyanide, thus connoting high efficiency and better economic boost. Finally, the Au-loaded A-OPAC was regenerated in a four-cycle adsorption-desorption studies using 1 M mixture of KCN and NaOH, making it potentially suitable for large-scale applications.

Credit authorship contribution statement

John Kwame Bediako: Conceptualization, Methodology, Data curation, Validation, Formal analysis, Investigation, Resources, Verification, Funding acquisition, Supervision, Writing – original draft, Writing – review & editing.

Declaration of competing interest

The author declares no known competing financial interest or personal relationship that could

View Article Online
DOI: 10.1039/D6CP00058D

have appeared to influence the work reported in this paper.

Data availability

Data will be made available on request.

Funding information

The author acknowledges financial supports from the Finnish Foundation for Soil and Water Engineering (No. 49854) and Erkki Paasikivi Foundation (No. 20250034).

Acknowledgements

The author expresses appreciation to Prof. Yeoung-Sang Yun of Jeonbuk National University (JBNU) for granting access to his laboratory, the Environmental Biotechnology National Research Lab (EBTL).

References

1. Britannica.com, https://www.britannica.com/technology/gold-processing/Mining-and-concentrating [Accessed: June 4, 2025 at 15:20].

2. Hough, R. M.; Butt, C. R. M.; Fischer-Bühner, J. , The crystallography, metallography and composition of gold. *Elements* **2009,** *5* (5), 297-302.

3. Msumange, D. A.; Yazıcı, E. Y.; Celep, O.; Deveci, H., The effectiveness of adsorbents for selective recovery of gold from copper-bearing cyanide leach solutions. *Bilimsel Madencilik Dergisi* **2021,** *60* (1), 21-30.

4. Li, Y.; Tian, H.; Xiao, C.; Ding, J.; Chen, X., Efficient recovery of precious metal based on Au–S bond and electrostatic interaction. *Green Chem.* **2014,** *16* (12), 4875-4878.

View Article Online
DOI: 10.1039/D6CP00058D

5. Ahamed, M. E. H.; Mbianda, X. Y.; Mulaba-Bafubiandi, A. F.; Marjanovic, L., Selective extraction of gold(III) from metal chloride mixtures using ethylenediamine N-(2-(1-imidazolyl)ethyl) chitosan ion-imprinted polymer. *Hydrometallurgy* **2013,** *140*, 1-13.

6. Lin, S.; Kumar Reddy, D. H.; Bediako, J. K.; Song, M.-H.; Wei, W.; Kim, J.-A.; Yun, Y.-S., Effective adsorption of Pd(II), Pt(IV) and Au(III) by Zr(iv)-based metal–organic frameworks from strongly acidic solutions. *J. Mater. Chem. A* **2017, (**26), 13557-13564.

7. Bediako, J. K., Effects of carbon precursors and activation agents on the physicochemical characteristics and aurocyanide adsorption patterns of agro waste-based activated carbons. *Result. Eng.* **2026,** *29*, 108715.

8. Jia, Y.; Thomas, K. M., Observation of the adsorption of $K^+Au(CN)_2^-$ ion pairs on the surface of nanoporous carbon by XANES. *J. Phys. Chem. B* **2004,** *108* (44), 17124-17128.

9. Lagerge, S.; Zajac, J.; Partyka, S.; Groszek, A. J., Comparative study on the adsorption of cyanide gold complexes onto different carbonaceous samples: measurement of the reversibility of the process and assessment of the active surface inferred by flow microcalorimetry. *Langmuir* **1999,** *15* (14), 4803-4811.

10. Yin, C.-Y.; Ng, M.-F.; Saunders, M.; Goh, B.-M.; Senanayake, G.; Sherwood, A.; Hampton, M., New insights into the adsorption of aurocyanide ion on activated carbon surface: electron microscopy analysis and computational studies using fullerene-like models. *Langmuir* **2014,** *30* (26), 7703-7709.

11. Rubina Acuna, C.; Oraby, E. A.; Bezuidenhout, G. A.; Beh, C. C.; Eksteen, J. J., Adsorption of Platinum from Alkaline Glycine–Cyanide Solutions Using Activated Carbon: Leachates, Water, and Waste Treatment Applications. *Separations* **2025,** *12* (10), 284.

12. Poinern, G. E. J.; Senanayake, G.; Shah, N.; Thi-Le, X. N.; Parkinson, G. M.; Fawcett, D., Adsorption of the aurocyanide, Au(CN)2- complex on granular activated carbons derived from macadamia nut shells – A preliminary study. *Miner. Eng.* **2011,** *24* (15), 1694-1702.

View Article Online
DOI: 10.1039/D6CP00058D

13. Hiremath, M. N.; Shivayogimath, C. B.; Shivalingappa, S. N., Preparation and characterization of granular activated carbon from corn cob by KOH activation. *Int. J. Res. Chem. Environ.* **2012,** *2* (3), 84-87.

14. Chand, R.; Watari, T.; Inoue, K.; Kawakita, H.; Luitel, H. N.; Parajuli, D.; Torikai, T.; Yada, M., Selective adsorption of precious metals from hydrochloric acid solutions using porous carbon prepared from barley straw and rice husk. *Miner. Eng.* **2009,** *22* (15), 1277-1282.

15. Soleimani, M.; Kaghazchi, T., Adsorption of gold ions from industrial wastewater using activated carbon derived from hard shell of apricot stones – an agricultural waste. *Bioresour. Technol.* **2008,** *99* (13), 5374-5383.

16. Soleimani, M.; Kaghazchi, T., Activated Hard Shell of Apricot Stones: A Promising Adsorbent in Gold Recovery. *Chinese J. Chem. Eng.* **2008,** *16* (1), 112-118.

17. Bediako, J. K.; Affrifah, N. S.; Yun, Y.-S.; Repo, E., Experimental optimization of aurocyanide adsorption onto biomass activated carbon and re-examination of the adsorption mechanisms. *Miner. Eng.* **2025,** *227*, 109293.

18. Unur, E., Functional nanoporous carbons from hydrothermally treated biomass for environmental purification. *Micropor. Mesopor. Mat.* **2013,** *168*, 92-101.

19. Yin, Q.; Zhang, B.; Wang, R.; Zhao, Z., Biochar as an adsorbent for inorganic nitrogen and phosphorus removal from water: a review. *Environ. Sci. Pollut. Res.* **2017,** *24* (34), 26297-26309.

20. Rafatullah, M.; Sulaiman, O.; Hashim, R.; Ahmad, A., Adsorption of methylene blue on low-cost adsorbents: A review. *J. Hazard. Mater.* **2010,** *177* (1–3), 70-80.

21. Zuo, X.; Liu, Z.; Chen, M., Effect of H_2O_2 concentrations on copper removal using the modified hydrothermal biochar. *Bioresour. Technol.* **2016,** *207*, 262-7.

22. Ahmed, M. J.; Dhedan, S. K., Equilibrium isotherms and kinetics modeling of methylene

View Article Online
DOI: 10.1039/D6CP00058D

552 blue adsorption on agricultural wastes-based activated carbons. *Fluid Phase Equil.* **2012,** *317*,
553 9-14.
554 23. Yahya, M. A.; Al-Qodah, Z.; Ngah, C. W. Z., Agricultural bio-waste materials as
555 potential sustainable precursors used for activated carbon production: a review. *Renew. Sust.*
556 *Energ. Rev.* **2015,** *46*, 218-235.
557 24. Wang, J.; Kaskel, S., KOH activation of carbon-based materials for energy storage. *J.*
558 *Mater. Chem.* **2012,** *22* (45), 23710-23725.
559 25. Sevilla, M.; Ferrero, G. A.; Fuertes, A. B., Beyond KOH activation for the synthesis of
560 superactivated carbons from hydrochar. *Carbon* **2017,** *114*, 50-58.
561 26. Park, J.; Hung, I.; Gan, Z.; Rojas, O. J.; Lim, K. H.; Park, S., Activated carbon from
562 biochar: Influence of its physicochemical properties on the sorption characteristics of
563 phenanthrene. *Bioresour. Technol.* **2013,** *149*, 383-389.
564 27. Wu, S.; Yan, P.; Yang, W.; Zhou, J.; Wang, H.; Che, L.; Zhu, P., ZnCl(2) enabled
565 synthesis of activated carbons from ion-exchange resin for efficient removal of Cu(2+) ions
566 from water via capacitive deionization. *Chemosphere* **2021,** *264* (Pt 2), 128557.
567 28. Cesano, F.; Cravanzola, S.; Brunella, V.; Scarano, D., Porous carbon spheres from
568 poly(4-ethylstyrene-co-divinylbenzene: role of ZnCl2 and KOH agents in affecting porosity,
569 surface area and mechanical properties. *Micropor. Mesopor. Mat.* **2019,** *288*, 109605.
570 29. Foo, K. Y.; Hameed, B. H., Preparation, characterization and evaluation of adsorptive
571 properties of orange peel based activated carbon via microwave induced K_2CO_3 activation.
572 *Bioresour. Technol.* **2012,** *104*, 679-686.
573 30. Zequine, C.; Ranaweera, C. K.; Wang, Z.; Dvornic, P. R.; Kahol, P. K.; Singh, S.;
574 Tripathi, P.; Srivastava, O. N.; Singh, S.; Gupta, B. K.; Gupta, G.; Gupta, R. K., High-
575 performance flexible supercapacitors obtained via recycled jute: bio-waste to energy storage
576 approach. *Sci. Rep.* **2017,** *7* (1), 1174.

View Article Online
DOI: 10.1039/D6CP00058D

31. Hayashi, J.; Yamamoto, N.; Horikawa, T.; Muroyama, K.; Gomes, V. G., Preparation and characterization of high-specific-surface-area activated carbons from K_2CO_3-treated waste polyurethane. *J. Colloid. Interf. Sci.* **2005,** *281* (2), 437-43.

32. Etale, A.; Nhlane, D. S.; Mosai, A. K.; Mhlongo, J.; Khan, A.; Rumbold, K.; Nuapia, Y. B., Synthesis and application of cationised cellulose for removal of Cr(VI) from acid mine-drainage contaminated water. *AAS Open Res* **2021,** *4*, 4.

33. Zhao, Y.; Li, Y.; Liu, X.; Huo, S.; Fang, J.; Liu, R.; Sun, C.; Xu, L.; Shen, X.; Geng, S.; Wang, J.; Li, K., The improvement of selective removal of nitrate using reactive cationic surfactant modified activated carbon in capacitive deionization. *Separation and Purification Technology* **2026,** *392*, 137188.

34. Wang, X.; Zhang, Y.; Li, J.; Zhang, G.; Li, X., Enhance Cr(VI) removal by quaternary amine-anchoring activated carbons. *J.Taiwan Inst. Chem. Eng.* **2016,** *58*, 434-440.

35. Vargas, C.; Navarro, P.; Mejía, E.; Hernández, P., Aurocyanide adsorption onto granular activated carbon impregnated with SDS anionic surfactant. *Gold Bulletin* **2022,** *55* (2), 137-143.

36. Ramirez-Muniz, K.; Song, S.; Berber-Mendoza, S.; Tong, S., Adsorption of the complex ion Au(CN)2- onto sulfur-impregnated activated carbon in aqueous solutions. *J. Colloid Interf. Sci.* **2010,** *349* (2), 602-6.

37. Armando, N.; Spreen, T. H.; Jauregui, C., The citrus industry of Cuba: 1994-1999. Forthcoming International Working Paper, Food and Resource Economics Department, University of Florida, Gainesville. **2001**.

38. Spreen, T. H., Projections of world production and consumption of citrus to 2010. FAO Corporate Document Repository, Economic and Social Development Department. http://www.fao.org/DOCREP/003/X6732E/x6732e 02.htm. **2010**.

39. Singh, R. P.; Pal, S.; Rana, V. K.; Ghorai, S., Amphoteric amylopectin: a novel polymeric

View Article Online
DOI: 10.1039/D6CP00058D

602 flocculant. *Carbohydr. Polym.* **2013,** *91* (1), 294-9.
603 40. Ferrero, F., Dye removal by low cost adsorbents: hazelnut shells in comparison with
604 wood sawdust. *J. Hazard. Mater.* **2007,** *142* (1-2), 144-52.
605 41. Bediako, J. K.; Kudoahor, E.; Lim, C. R.; Affrifah, N. S.; Kim, S.; Song, M. H.; Repo, E.,
606 Exploring the insights and benefits of biomass-derived sulfuric acid activated carbon for
607 selective recovery of gold from simulated waste streams. *Waste Manag* **2024,** *177*, 135-145.
608 42. Bediako, J. K.; Reddy, D. H. K.; Song, M.-H.; Wei, W.; Lin, S.; Yun, Y.-S., Preparation,
609 characterization and lead adsorption study of tripolyphosphate-modified waste Lyocell fibers.
610 *J. Env. Chem. Eng.* **2017,** *5* (1), 412-421.
611 43. Ramraj, S. M.; Kubaib, A.; Imran, P. M.; Thirupathy, M. K., Utilizing Sida Acuta leaves
612 for low-cost adsorption of chromium (VI) heavy metal with activated charcoal. *J. Hazard.*
613 *Mater. Adv.* **2023,** *11*, 100338.
614 44. Moreno-Tovar, R.; Terrés, E.; Rangel-Mendez, J. R., Oxidation and EDX elemental
615 mapping characterization of an ordered mesoporous carbon: Pb(II) and Cd(II) removal. *Appl.*
616 *Surf. Sci.* **2014,** *303*, 373-380.
617 45. Khan, M.; Shafi, M.; Raza, J.; Ahmed, I. A.; Zada, A.; Narasimharao, K.; Sun, X.,
618 Mechanistic breakthroughs in affordable adsorbents for heavy metal remediation: An in-
619 depth exploration of next-generation sustainable water purification technologies. *J. Hazard.*
620 *Mater. Adv.* **2025,** *19*, 100847.
621 46. Huang, W.; Zhang, H.; Huang, Y.; Wang, W.; Wei, S., Hierarchical porous carbon
622 obtained from animal bone and evaluation in electric double-layer capacitors. *Carbon* **2011,**
623 *49* (3), 838-843.
624 47. Chen, W.; Zhang, H.; Huang, Y.; Wang, W., A fish scale based hierarchical lamellar
625 porous carbon material obtained using a natural template for high performance
626 electrochemical capacitors. *J. Mater. Chem.* **2010,** *20* (23), 4773-4775.

View Article Online
DOI: 10.1039/D6CP00058D

627 48. Nekouei, F.; Kargarzadeh, H.; Nekouei, S.; Tyagi, I.; Agarwal, S.; Kumar Gupta, V.,
628 Preparation of nickel hydroxide nanoplates modified activated carbon for malachite green
629 removal from solutions: kinetic, thermodynamic, isotherm and antibacterial studies. *Process*
630 *Saf. Environ. Prot.* **2016,** *102*, 85-97.
631 49. Sun, G.; Li, X.; Qu, Y.; Wang, X.; Yan, H.; Zhang, Y., Preparation and characterization
632 of graphite nanosheets from detonation technique. *Mater. Lett.* **2008,** *62* (4-5), 703-706.
633 50. Jones, W.; Klauber, C.; Linge, H. G., Randol Conf. on Gold and Silver, Perth, Australia,
634 1988, Randol International, Golden, CO **1988**, 243-248.
635 51. Cazorla-Amoros, D.; Alcaniz-Monge, J.; Linares-Solano, A., Characterization of
636 activated carbon fibers by CO_2 adsorption. *Langmuir* **1996,** *12*.
637 52. Qi, J.; Zhang, W.; Xiang, R.; Liu, K.; Wang, H. Y.; Chen, M.; Han, Y.; Cao, R., Porous
638 nickel-iron oxide as a highly efficient electrocatalyst for oxygen evolution reaction. *Adv. Sci.*
639 *(Weinh)* **2015,** *2* (10), 1500199.
640 53. Khalfaoui, M.; Knani, S.; Hachicha, M. A.; Lamine, A. B., New theoretical expressions
641 for the five adsorption type isotherms classified by BET based on statistical physics
642 treatment. *J. Colloid Interf. Sci.* **2003,** *263* (2), 350-356.
643 54. de Carvalho, H. P.; Huang, J.; Zhao, M.; Liu, G.; Dong, L.; Liu, X., Improvement of
644 methylene blue removal by electrocoagulation/banana peel adsorption coupling in a batch
645 system. *Alex. Eng. J.* **2015,** *54* (3), 777-786.
646 55. Chen, Y.; Zhai, S.-R.; Liu, N.; Song, Y.; An, Q.-D.; Song, X.-W., Dye removal of
647 activated carbons prepared from NaOH-pretreated rice husks by low-temperature solution-
648 processed carbonization and H_3PO_4 activation. *Bioresour. Technol.* **2013,** *144*, 401-409.
649 56. Wang, Y.; Liu, X.; Wang, H.; Xia, G.; Huang, W.; Song, R., Microporous spongy
650 chitosan monoliths doped with graphene oxide as highly effective adsorbent for methyl
651 orange and copper nitrate ($Cu(NO_3)_2$) ions. *J. Colloid Interf. Sci.* **2014,** *416*, 243-251.

View Article Online
DOI: 10.1039/D6CP00058D

652 57. Zhang, S.; Wang, Z.; Chen, H.; Kai, C.; Jiang, M.; Wang, Q.; Zhou, Z., Polyethylenimine
653 functionalized Fe_3O_4/steam-exploded rice straw composite as an efficient adsorbent for
654 Cr(VI) removal. *Appl. Surf. Sci.* **2018,** *440*, 1277-1285.
655 58. Valle-Vigon, P.; Sevilla, M.; Fuertes, A. B., Carboxyl-functionalized mesoporous silica-
656 carbon composites as highly efficient adsorbents in liquid phase. *Micropor. Mesopor. Mat.*
657 **2013,** *176*, 78-85.
658 59. Sui, Z. Y.; Cui, Y.; Zhu, J. H.; Han, B. H., Preparation of three-dimensional graphene
659 oxide-polyethylenimine porous materials as dye and gas adsorbents. *ACS Appl. Mater.*
660 *Interfaces* **2013,** *5* (18), 9172-9.
661 60. Yan, Y.; An, Q.; Xiao, Z.; Zheng, W.; Zhai, S., Flexible core-shell/bead-like
662 alginate@PEI with exceptional adsorption capacity, recycling performance toward batch and
663 column sorption of Cr(VI). *Chem. Eng. J.* **2017,** *313*, 475-486.
664 61. Klauber, C., X-ray photoelectron spectroscopic study of the adsorption mechanism of
665 aurocyanide onto activated carbon. *Langmuir* **1991,** *7* (10), 2153-2159.
666 62. Van Deventer, J. S. J.; Van Der Merwe, P. F., The reversibility of adsorption of gold
667 cyanide on activated carbon. *Metall. Mater. Trans. B* **1993,** *24* (3), 433-440.
668 63. Ibrado, A. S.; Fuerstenau, D. W., Infrared and X-ray photoelectron spectroscopy studies
669 on the adsorption of gold cyanide on activated carbon. *Miner. Eng.* **1995,** *8* (4–5), 441-458.
670 64. Majumdar, A.; Das, S. C.; Shripathi, T.; Hippler, R. J. C. I., Chemical synthesis and
671 surface morphology of amorphous hydrogenated carbon nitride film deposited by N2/CH4
672 dielectric barrier discharge plasma. **2012,** *19* (3-4), 161-170.
673 65. Ech-chamikh, E.; Essafti, A.; Ijdiyaou, Y.; Azizan, M., XPS study of amorphous carbon
674 nitride (a-C:N) thin films deposited by reactive RF sputtering. *Sol. Energy Mater. Sol. Cells*
675 **2006,** (90), 1420–1423.
676 66. Beshkov, G.; Dimitrov, D. B.; Georgiev, S.; Juan-Cheng, D.; Petrov, P.; Velchev, N.;

View Article Online
DOI: 10.1039/D6CP00058D

677 Krastev, V., XPS spectra of thin CN films prepared by chemical vapor deposition. *Diam.*
678 *Relat. Mater.* **1999,** (8), 591–594.
679 67. Portal, L.; Polishchuk, I.; Zilberberg, R.; Levi, M.; Koifman-Khristosov, M.; Katsman,
680 A.; Pokroy, B., Deformation twin traces on gold surfaces: A pathway to tailored epitaxial
681 growth of 1D semiconductors. *Proc. Natl. Acad. Sci. U. S. A.* **2023,** *120* (50), e2314192120.
682 68. Moulder, J. F.; Stickle, W. F.; Sobol, P. E.; Bomben, K. D., *Handbook of X-ray*
683 *photoelectron spectroscopy: A reference book of standard spectra for identification and*
684 *interpretation of XPS data*. Perkin-Elmer Corporation, Physical Electronics Division: 6509
685 Flying Cloud Drive, Eden Prairie, Minnesota 55344 U.S.A., 1992.
686 69. Radnik, J.; Mohr, C.; Claus, P., On the origin of binding energy shifts of core levels of
687 supported gold nanoparticles and dependence of pretreatment and material synthesis. *Phys.*
688 *Chem. Chem. Phys.* **2003,** *5* (1), 172-177.
689 70. Sankar, M.; He, Q.; Morad, M.; Pritchard, J.; Freakley, S. J.; Edwards, J. K.; Taylor, S.
690 H.; Morgan, D. J.; Carley, A. F.; Knight, D. W.; Kiely, C. J.; Hutchings, G. J., Synthesis of
691 Stable Ligand-free Gold–Palladium Nanoparticles Using a Simple Excess Anion Method.
692 *ACS Nano* **2012,** *6* (8), 6600-6613.
693 71. Pinto, P. I. F.; Magina, S.; Budjav, E.; Pinto, P. C. R.; Liebner, F.; Evtuguin, D.,
694 Cationization of Eucalyptus Kraft LignoBoost Lignin: Preparation, Properties, and Potential
695 Applications. *Ind. Eng. Chem. Res.* **2022,** *61* (10), 3503-3515.
696 72. Fernandes, C.; Gomes, L. C.; Bernin, D.; Alves, L.; Medronho, B.; Rasteiro, M. G.;
697 Varela, C., Optimizing lignin cationization: Unveiling the impact of reaction conditions
698 through multi-response analysis. *Chem. Eng. J.* **2025,** *522*, 167345.
699 73. Sina Ghasemi; Sima Mohammadnejad; Khalesi, M. R., Role of functional groups in
700 selective adsorption of gold over copper cyano complexes by activated carbon: A DFT study.
701 *J. Min. Environ.* **2022,** *13* (3), 891-901.

View Article Online
DOI: 10.1039/D6CP00058D

74. Liu, Y.; Wang, J.; Zheng, Y.; Wang, A., Adsorption of methylene blue by kapok fiber treated by sodium chlorite optimized with response surface methodology. *Chem. Eng. J.* **2012,** *184*, 248-255.

75. Park, S. W.; Bediako, J. K.; Song, M.-H.; Choi, J.-W.; Lee, H.-C.; Yun, Y.-S., Facile fabrication of polyacrylic acid-polyvinyl chloride composite adsorbents for the treatment of cadmium-contaminated wastewater. *J. Env. Chem. Eng.* **2018,** *6* (2), 2401-2408.

76. Lagergren, S., Zur theorie der sogenannten adsorption gelöster stoffe. . *Kungl. Svensk. Vetensk. Handl.* **1898,** *24* (4), 1-39.

77. Ho, Y. S.; McKay, G., Pseudo-second order model for sorption processes. *Process Biochem.* **1999,** *34*, 451-465.

78. Borah, D.; Satokawa, S.; Kato, S.; Kojima, T., Sorption of As(V) from aqueous solution using acid modified carbon black. *J. Hazard. Mater.* **2009,** *162* (2-3), 1269-77.

79. Weber, W. J.; Moris, J. C., Kinetics of adsorption on carbon from solution. *J. Sanit. Eng. Div. Am. Soc. Civ. Eng.* **1963,** *89*, 31-60.

80. Kim, M. H.; Hwang, C.-H.; Kang, S. B.; Kim, S.; Park, S. W.; Yun, Y.-S.; Won, S. W., Removal of hydrolyzed Reactive Black 5 from aqueous solution using a polyethylenimine–polyvinyl chloride composite fiber. *Chem. Eng. J.* **2015,** *280* (0), 18-25.

81. Buah, W. K.; Williams, P. T., Granular activated carbons from palm nut shells for gold di-cyanide adsorption. *Int. J. Miner. Metall. Mater.* **2013,** *20* (2), 172-179.

82. Xia, J.; Mahandra, H.; Ghahreman, A., Efficient Gold Recovery from Cyanide Solution Using Magnetic Activated Carbon. *ACS Appl. Mater. Interfaces* **2021,** *13* (40), 47642-47649.

83. Bediako, J. K.; Yun, Y.-S., Adsorption of aurocyanide onto KOH-activated orange peel carbons: optimisation of the activated carbon yield and adsorption capacity through central composite design. In *5th UMaT Biennial International Mining and Mineral Conference*, *Ghana Min. J.*: UMaT, Tarkwa, Ghana, 2018; pp. MR62-67.

View Article Online
DOI: 10.1039/D6CP00058D

84. Maponga, T. C.; Mahamadi, C., Efficient Au(CN)2- adsorption using peach stone-derived granular activated carbon. *Sci. Rep.* **2019,** *9* (1), 3373.

85. Martínez-Mendoza, K. L.; Barraza Burgos, J. M.; Marriaga-Cabrales, N.; Machuca-Martinez, F.; Barajas, M.; Romero, M., Production and Characterization of Activated Carbon from Coal for Gold Adsorption in Cyanide Solutions. *Ingeniería e Investigación* **2020,** *40* (1), 34-44.

86. Tian, Y.; Wu, M.; Liu, R.; Wang, D.; Lin, X.; Liu, W.; Ma, L.; Li, Y.; Huang, Y., Modified native cellulose fibers—A novel efficient adsorbent for both fluoride and arsenic. *J. Hazard. Meter.* **2011,** *185* (1), 93-100.

87. Langmuir, I., The adsorption of gases on plane surfaces of glass, mica and platinum. *J. Am. Chem. Soc.* **1918,** *40* (9), 1361-1403.

88. Freundlich, H. M. F., Über die Adsorption in Lösungen. *Z. Phys. Chem.* **1906,** *A* (57), 385-470.

89. Erdem, E.; Karapinar, N.; Donat, R., The removal of heavy metal cations by natural zeolites. *J. Colloid Interf. Sci.* **2004,** *280* (2), 309-14.

Data Availability Statement

View Article Online
DOI: 10.1039/D6CP00058D

Data will be made available on request.